

# Optimization of Hot Forming-Quenching Integrated Process Parameters for Complex Aluminum Alloy Automotive Components

Li Huanhuan<sup>1,2,3</sup>, Hu Zhili<sup>2,3</sup>, Hua Lin<sup>1,2,3</sup>, Chen Yizhe<sup>2,3</sup>

<sup>1</sup> School of Materials Science and Engineering, Wuhan University of Technology, Wuhan 430070, China; <sup>2</sup> Hubei Key Laboratory of Advanced Technology for Automotive Components, Wuhan University of Technology, Wuhan 430070, China; <sup>3</sup> Hubei Collaborative Innovation Center for Automotive Components Technology, Wuhan University of Technology, Wuhan 430070, China

**Abstract:** To obtain appropriate forming parameters, a thermo-mechanical finite element (FE) model using a unified viscoplastic damage model was set up to predict the formability of a complex-designed 6xxx aluminum alloy B-pillar. A back propagation (BP) neural-network combined with multi-objective genetic algorithm (GA) method was adopted to optimize the key process variables including blank temperature, stamping speed and die clearance during hot stamping process. The results show that after optimization, the thinning and thickening rates are reduced to 13.0% and 10.0% compared with the initial 56.5% and 14.2%, respectively. In addition, a successful hot stamping B-pillar with satisfactory mechanical performance and excellent forming accuracy is achieved experimentally using the optimized parameters, indicating that the finite element model can simulate the hot stamping process accurately, and that the optimization method utilized in this paper is feasible and effective.

**Key words:** hot stamping; unified viscoplastic damage constitutive equation; BP artificial neural network; multi-objective optimization

Recently, vehicle lightweighting has become an urgent matter for achieving energy saving and environment protection. Aluminum alloys exhibit bright prospects in vehicle lightweight industry with a capability of high specific strength, super corrosion resistance and recycling<sup>[1,2]</sup>. However, further applications of aluminum alloys are restricted due to the poor formability and inevitable springback during the forming processes at room temperature<sup>[3-5]</sup>. It is known that the formability of the aluminum alloys increases with increasing the forming temperature<sup>[6,7]</sup>. Therefore, many forming techniques have been carried out at elevated temperature, such as warm forming, superplastic forming, warm hydroforming and hot metal gas forming. Nevertheless, these techniques mentioned above are far from satisfactory because the high cost, low efficiency and less accuracy are the main issues for the volume production of aluminum alloy automotive components<sup>[8,9]</sup>.

Aluminum alloy hot stamping is firstly proposed by Lin<sup>[10]</sup>,

which combines the forming and quenching into one operation. Firstly, the aluminum alloy sheet was held at its solution heat temperature (SHT) for a certain period to obtain a supersaturated solid solution (SSS), and then the SSSed sheet was transferred into cold stamping dies while being formed and quenched for several seconds. Artificial aging was finally carried out within 2 h to obtain full strength. Hot stamping is one of the most promising forming techniques for the mass production of complex shaped profiles with satisfactory formability and excellent accuracy<sup>[11-13]</sup>. Much attention has been paid to this novel aluminum alloy forming process. Fan et al<sup>[14,15]</sup> investigated the effect of temperature and solution time on the mechanical properties of AA6082, and it is shown that the Vickers hardness improves significantly with increasing the solution time after artificial aging (<50 min). Moreover, the strengthening mechanism is revealed. The hot stamping speed plays an important role in the formability of

Received date: April 28, 2018

Foundation item: National Natural Science Foundation of China (U1564202, 51405358, 51775397); "111" Project (B17034); Innovative Research Team Development Program of Ministry of Education of China (IRT13087)

Corresponding author: Hua Lin, Ph. D., Professor, Hubei Key Laboratory of Advanced Technology for Automotive Components, Wuhan University of Technology, Wuhan 430070, P. R. China, Tel: 0086-27-87168391, E-mail: hualin@whut.edu.cn

Copyright © 2019, Northwest Institute for Nonferrous Metal Research. Published by Science Press. All rights reserved.

AA2024 due to the fact that the speed determines the deformation rate and the temperature distribution of the sheet<sup>[16]</sup>. Ma et al<sup>[17]</sup> studied the impact of friction on the thickness uniformity and failure modes during hot forming of AA6111. However, until recently, almost all the investigations are concentrated on the fundamental understanding of the influence of solution heat treatment and single process parameter on the formability or mechanical properties. Besides, nearly all the researches focus on the simple parts, such as cylindrical parts, U-shaped parts and box-shaped parts.

Hot stamping process is a high combination of mechanical, thermal and microstructural fields, so that there are various and interactive process parameters that will influence the formability. Furthermore, automotive components are usually characterized by large size and complex-designed shape, which makes it difficult to ensure the formability and dimensional accuracy. Unreasonable process parameters can easily result in part invalidity including local rupture, wrinkle, springback or distortion. Hence, it has a very important practical significance to comprehensively optimize multiple parameters for improving the quality of hot stamping part. Existing researches on hot stamping process are focused mainly on the high strength steel. Researches on aluminum alloy are restricted due to the difficulty in controlling microstructure and properties. Zhou et al<sup>[18]</sup> presented a multi-objective optimization method for an aluminum alloy anti-collision side beam during hot stamping process. Xiao et al<sup>[19]</sup> proposed an efficient method to obtain optimal process parameters for a car front floor passage by integrating response surface methodology (RSM) and genetic algorithm. The aforementioned researches have accomplished the purpose of improving the quality of the aluminum alloy parts by optimizing the process parameters. However, studies on a clear mathematical model and a systematical optimization are

still required during hot stamping of aluminum alloy. BP neural network is often used to construct the mathematical relation between process parameters and optimization objectives owing to its powerful ability of nonlinear interpolation and self-learning. Genetic algorithm (GA) shows perfect performance in solving nonlinear multi-objective optimization mathematical model. The BP-GA method is proposed to address the optimization of process parameters during hot stamping of aluminum alloy. It is critical to carry out study in this area to offer industry application guidance.

In this work, in order to improve the formability of aluminum alloy during hot stamping of complex automotive components, hot tension tests at different temperatures (350, 450, and 520 °C) and different strain rates (0.01, 0.1, and 1 s<sup>-1</sup>) were carried out to investigate the rheological behavior of AA6061. A unified viscoplastic damage model according to damage mechanism was obtained and applied to non-isothermal FE model of a complex-designed automotive part using commercial software LS-DYNA. The combination of BP and GA was used to optimize three main hot forming parameters, namely blank temperature, stamping speed and die clearance. At last, an eligible aluminum alloy B pillar was gained by employing the optimal parameters. It is a demonstration of the FE models and the reliability of this optimization method, and also provides guidance for actual production.

## 1 Material and Simulation

### 1.1 Materials

The as-received material is 6061-O aluminum alloy with 1.6 mm in thickness. Table 1 shows the performance at room temperature. The thermal physical properties<sup>[20,21]</sup> needed in FE simulation of 6061 hot forming are shown in Table 2 and Fig.1, including thermal conductivity, specific heat, and thermal expansion coefficient at different temperatures.

**Table 1 Mechanical properties of AA6061 at room temperature**

Density/kg·m <sup>-3</sup>	Poisson's ratio	Modulus/GPa	Elongation/%	$\sigma_s$ /MPa	$\sigma_b$ /MPa
2700	0.33	68.9	25	55.2	124

**Table 2 Mean coefficient of thermal expansion (CTE) of AA6061 at different temperatures ( $\times 10^{-6} \text{ }^\circ\text{C}^{-1}$ )**

25~100 °C	25~200 °C	25~300 °C	25~400 °C	25~500 °C
23.4	24.3	25.3	25.4	25.5

### 1.2 Material model for AA6061 hot stamping

It is an undeniable fact that the flow stress increases significantly with the increase of strain rate for aluminum alloys at high temperatures. This is the result of the mixed effects of high temperature creep, recovery and other mechanisms, which needs a unified viscoplastic theory to minimize the error of the modeling<sup>[22]</sup>. The material model implemented in this study is the unified viscoplastic damage constitutive equations considering both the dislocation density and the damage effect

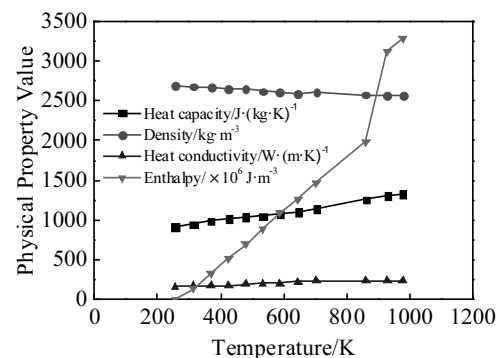


Fig.1 Physical properties of AA6061 at different temperatures

proposed by Mohamed et al<sup>[23,24]</sup>, which are represented as follows:

$$\left\{ \begin{array}{l} \dot{\varepsilon}_p = \left( \frac{\sigma}{(1-f_d)} - R - k \right)^{n_1} \\ R = B\bar{\rho}^{1/2} \\ \dot{\bar{\rho}} = A(1-\bar{\rho})|\dot{\varepsilon}_p| - C\bar{\rho}^{n_2} \\ \dot{f}_d = \frac{D_1\dot{\varepsilon}_p^{d_1}}{(1-f_d)^{d_2}} \sinh(D_2\varepsilon_p) \\ \sigma = E(1-f_d)(\varepsilon_T - \varepsilon_p) \end{array} \right. \quad (1) \quad \left\{ \begin{array}{l} K = K_0 \exp\left(\frac{Q_K}{R_g T}\right) \\ k = k_0 \exp\left(\frac{Q_k}{R_g T}\right) \\ B = B_0 \exp\left(\frac{Q_B}{R_g T}\right) \\ C = C_0 \exp\left(-\frac{Q_C}{R_g T}\right) \\ E = E_0 \exp\left(\frac{Q_E}{R_g T}\right) \\ D_1 = D_{10} \exp\left(\frac{Q_{D1}}{R_g T}\right) \end{array} \right. \quad (2)$$

where  $K_0, k_0, B_0, C_0, E_0, D_{10}$  are the equation coefficients,  $Q_K, Q_k, Q_B, Q_C, Q_E, Q_{D1}$  are the corresponding activation energy,  $R_g$  is the universal gas constant, and  $T$  is the absolute deformation temperature;  $\bar{\rho}$  is the normalized dislocation density which varies from 0 to 1;  $\dot{f}_d$  is the damage rate,  $f_d$  is the damage parameter;  $\dot{\varepsilon}$  is the strain rate, and  $\varepsilon_e, \varepsilon_T, \varepsilon_p$  are the elastic, total, and plastic strain, respectively;  $d_1, d_2, D_2, A, n_2$  are the non-temperature-dependent material constants;  $R$  is the material hardening,  $k$  is the initial yield stress,  $n_1$  is material constant,  $E$  is the Young's modulus, and  $\sigma$  is the flow stress.

This model consists of highly non-linear and interconnected ordinary differential equations with a total of 18 material constants, which are very difficult to determine using the traditional algebraic method. The GA technique is used for searching the suitable values owing to its accuracy and efficiency. The determined material constants are listed in Table 3, and then the results of predicting stress-strain relationships (solid curves) corresponding to the experimental data (symbols) are shown in Fig.2. It can be clearly seen that nice agreements are achieved for all, indicating that these material constants obtained are reasonable, and that this constitutive equation is available for well modeling of AA6061 hot deformation behavior.

### 1.3 FE model

The geometry and FE model of a complex automotive component (B pillar) are shown in Fig.3. The model consists of upper die, lower die, binder and aluminum alloy sheet, all of which are defined as shell element. The dies and binder are regarded as a rigid body without considering deformation, whose temperature was set as 25 °C. When the material is fully solid heat treated, the anisotropic material becomes isotropic<sup>[14,23]</sup>. The yield criterion Barlat89 was employed in this

FE model, and the 6\*MAT\_THERMAL\_ISOTROPIC\_TD\_LC was selected to define the thermal properties varied with temperatures for better characterization of the 6061 hot forming performance<sup>[25]</sup>. Both the simulation and corresponding experiment result of the B pillar under the same initial stamping conditions: blank temperature are given in Fig.4 400 °C, stamping speed 300 mm/s and the clearance 0.

Thickness is an important index for evaluating the forming quality. The excessive thinning indicates the crack and the surplus thickening reveals the wrinkling in forming process<sup>[26]</sup>. From Fig.4, the 56.5% thinning severely exceeds the requirement known as 30% for car panels, which is considered to be a rupture defect. Both the simulation and experiment of B pillar show cracks under the initial conditions because large thinning occurred in the hot stamping process (see Fig.4). On the one hand, the blank plasticity improves with increasing the forming temperature, which is beneficial for the improvement of formability. On the other hand, however, the lower stress level and the smaller deformation resistance at elevated temperature easily lead to local thinning and failure on the left side wall of the B pillar. Stamping speed determines the deformation rate, influences the temperature distribution of the blank, and finally affects the formability. It is difficult for material to flow if the die clearance is too narrow, which causes excessive thinning of the side wall. All above may result in poor formability of B pillar under initial conditions. In addition, the simulation results are in good agreement with the experimental results, indicating that the FE model can correctly provide training samples for the subsequent BP neural network, which improves the efficiency of process parameters optimization and saves costs.

## 2 Optimization of Hot Stamping Process Parameters Based on the BP/GA Method

Hot stamping process is a combination of mechanical, thermal and microstructural fields, so there are various and interactive process parameters which will influence the part formability. There are many parameters determining the thermal field in AA6061 hot stamping, such as radiation, heat conduction, and thermal convection between the heated blank and the ambient, the heated blank and tools, and the tools and the cooling water, as well as the blank deformation and friction. The blank temperature changes and the material flow response changes. Temperature and strain decide the final microstructure and mechanical properties<sup>[27]</sup> of the hot stamped B pillar. Consequently, it is extremely important to explore the relationship between the formability and the process parameters.

Table 3 Mechanical properties of AA6061 at room temperature

$K_0/$	$k_0/$	$B_0/$	$C_0/$	$E_0/$	$Q_K/$	$Q_k/$	$Q_B/$	$Q_C/$	$Q_E/$	$A$	$n_1$	$n_2$	$D_{10}/$	$Q_{D1}/$	$d_1$	$d_2$	$D_2$
MPa	MPa	MPa	MPa	MPa	J·mol <sup>-1</sup>				MPa	J·mol <sup>-1</sup>							
6.2	4.1	0.55	270.2	1218.4	8717.8	200.2	26317.9	38965.5	8889.2	3.8	5.4	6.1	0.1	8550.4	0.95	0.6	2.5

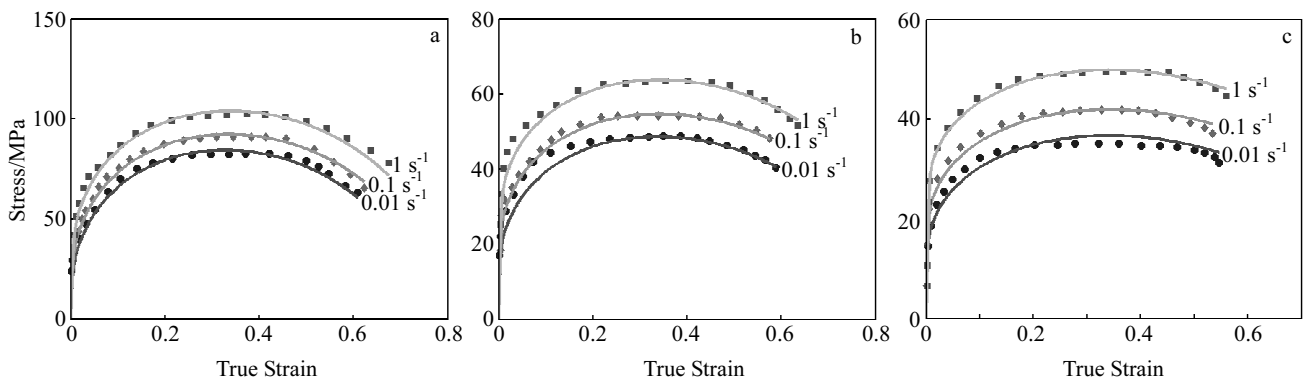


Fig.2 Comparison of predicted (solid curves) and experimental (symbols) stress-strain relationships for AA6061 at different temperatures and strain rates: (a) 350 °C, (b) 450 °C, and (c) 520 °C

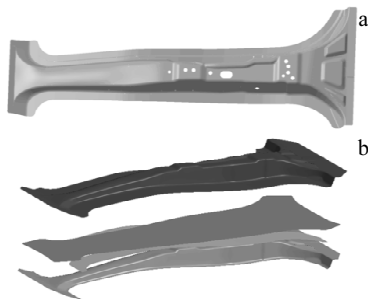


Fig.3 Geometry (a) and FE model (b) of B pillar

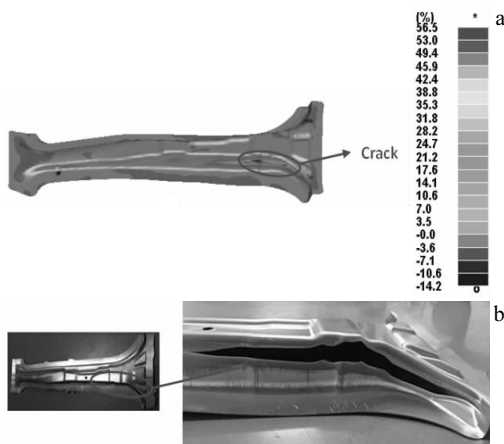


Fig.4 Hot forming of B pillar under initial conditions: (a) finite element simulation and (b) experiment

BP neural network integrated with GA has the powerful ability to deal with the nonlinear mathematical mapping reflecting the internal law of the experimental data, and has been widely used in engineering application for the prediction and optimization [28-31]. Considering blank temperature, stamping speed and die clearance, the maximum thinning and

thickening are taken as the objectives, and the orthogonal experimental design method was used to conduct the FE simulations. The BP and GA method were adopted to search the optimal process parameters. The network consists of one input layer with three neurons standing for blank temperature, stamping speed and clearance, one hidden layer with 11 neurons, and one output layer with two neurons representing thinning rate and thickening rate of B pillar. The setting of the processing parameters and results can be seen in Table 4.

The mean square error (MSE) was selected as the performance criterion for the BP neural network, which can be calculated by the following equation:

$$MSE = \left( \frac{1}{N} \sum_{i=1}^N |E_i - P_i| \right)^2 \tag{3}$$

where  $N$  is the amount of samples,  $E_i$  is the experimental value, and  $P_i$  is the corresponding prediction value. The smaller the MSE, the better the capability of the network. Fig.5 shows the training process of the BP neural network. The training curve illustrates that the mean square error declines gradually and converges to 0.0002 interminably within 7317 epochs, indicating that this prediction system has an accurate and rapid performance. The mathematic reflection between the process parameters and the formability is stored in the trained net, and the mathematic function is as follows:

$$W = f^1(\sum \omega_2 f^s(\omega_1 X)) \tag{4}$$

where  $W$  is the thinning rate and thickening rate of the B pillar;  $X = [x_1, x_2, x_3]^T$  indicates the values of blank temperature, stamping speed and clearance, respectively;  $f^s$  is the transfer function between input layer and hidden layer;  $f^1$  is the liner transfer function between hidden layer and output layer;  $\omega_1$  and  $\omega_2$  represent the connection weights between input layer and hidden layer, and hidden layer and output layer, respectively. In the GA optimization process, the population size, the mutation rate, the crossover rate and the generation size are set as 100, 0.1, 0.5 and 60, respectively.

In view of key process variables including blank temperature,

**Table 4 Orthogonal experimental design**

No.	Process parameters			Results	
	Blank temperature/°C	Stamping speed/mm·s <sup>-1</sup>	Clearance/mm	Thinning (max)/%	Thickening (max)/%
1	300	150	1.6	15.73	11.84
2	300	200	1.68	15.90	13.75
3	300	250	1.76	15.99	13.02
4	300	300	1.84	15.01	13.31
5	350	150	1.68	15.77	13.98
6	350	200	1.6	17.72	18.47
7	350	250	1.84	15.35	12.13
8	350	300	1.76	15.04	13.25
9	400	150	1.76	14.79	12.62
10	400	200	1.84	14.41	10.70
11	400	250	1.6	15.29	11.72
12	400	300	1.68	16.79	14.35
13	450	150	1.84	17.93	18.41
14	450	200	1.76	18.15	15.79
15	450	250	1.68	18.67	18.11
16	450	300	1.6	23.34	22.07

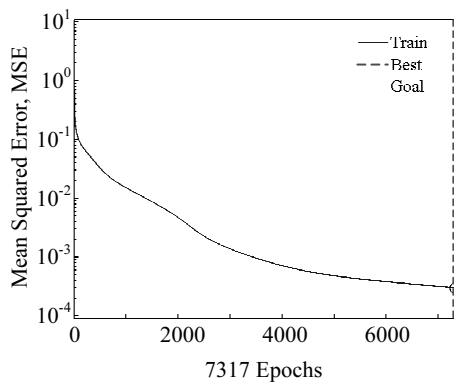


Fig.5 Training process of the network

stamping speed and clearance, a set of Pareto solutions based on multi-objective optimization genetic algorithm can be obtained. The final optimal process parameters are decided by the evaluation of satisfaction:

$$S = \frac{f_1 - f_{1\min}}{f_{1\max} - f_{1\min}} + \frac{f_2 - f_{2\min}}{f_{2\max} - f_{2\min}} \quad (5)$$

where  $f_{1\max}$  and  $f_{1\min}$  are the maximum and the minimum value of the first one objective in Pareto set, respectively;  $f_{2\max}$  and  $f_{2\min}$  are the maximum and the minimum value of the second one objective in Pareto set, respectively;  $S$  is the value of satisfaction, and the smaller, the better. Each value of  $S$  is calculated according to Eq.(5). Results show that the smallest  $S$  value appears under the following conditions: a blank temperature of 386 °C, a stamping speed of 268 mm/s, and a clearance of 1.84 mm.

### 3 Verification

On the purpose of estimating the precision of the FE model and the reliability of the optimization parameters based on the

BP and GA, the simulation result and the experiment result under optimized parameters are compared in this part. The actual B pillar hot stamping process is as follows: heating the AA6061 to its solution temperature of 520 °C and holding for 20 min; transferring the blank to the cold die by the robot system immediately, then hot stamping at a stamping speed of 268 mm/s when the blank temperature is 386 °C, and cooling synchronously in the cold die.

Under the optimized hot stamping parameters, the maximum thinning and the maximum thickening using optimized parameters in simulation are 13.0% and 10.0%, respectively. The relative error of thinning between the simulation and the BP neural network prediction is just 7.6%, and the relative error of thickening is only 0.2% (see Table 5). A Doppler ultrasound detector was used to measure the thickness of 30 points on the section A-A, which are 230 mm away from the bottom of bulge in horizontal direction. The points are extracted every 10 mm from the right side edge of the B pillar, and the thicknesses of 30 points for simulation and experiment are given in Fig.6. It can be seen from Fig.6 that the FE simulation is in good agreement with the experiment using the optimized parameters. The maximum relative error 1.9% appears at test point 11, and the possible reason is that point 11 is close to the fillet so it is difficult to detect accurately for the ultrasonic detector. Besides, the maximum thinning decreases from initial 56.5% to 13.0%, the thickening declines from 14.2% to 10.0%, indicating that the formability is greatly improved (see Table 6).

One of the most concerned issues is whether the mechanical properties of a successfully formed part in this forming process are comparable to those of 6061-T6. Three uniaxial tensile specimens (according to GB/T 228.1-2010) were cut from different locations and tested for mechanical property evaluation. Engineering stress-strain curves of these three

**Table 5 Comparison between numerical simulation and optimization results**

Index	Thinning (max)/%	Thickening (max)/%	Break	Wrinkle
Simulation	13.0	10.0	No	No
Optimization	12.01	10.02	No	No
Relative error/%	7.6	0.2		

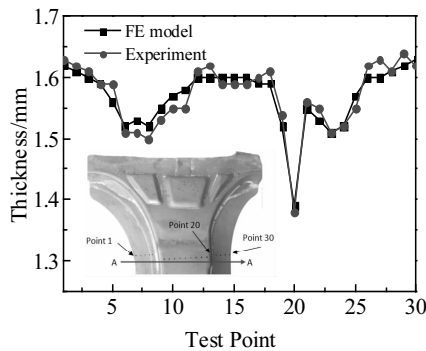


Fig.6 Thickness of test points on section A-A

**Table 6 Comparison of simulation results before and after optimization**

Index	Thinning (max)/%	Thickening (max)/%	Break	Wrinkle
Before	56.5	14.2	Yes	No
After	13.0	10.0	No	No

tensile specimens are shown in Fig.7. It can be seen that the ultimate strengths range from 300 MPa to 320 MPa, which is consistent with that of 6061-T6 aluminum alloy<sup>[32]</sup>. It is demonstrated that the performance of the parts formed using the optimized process parameters can meet the requirements. The strength distribution of the formed B-pillar is also relatively uniform.

In addition, the springback of the trimmed hot stamped B pillar is measured using a blue light scanner. All measured values at different points are within  $\pm 0.8$  mm, which can meet the requirements of vehicle industry. The accuracy of dimensions is also improved compared to 1.5 mm of the

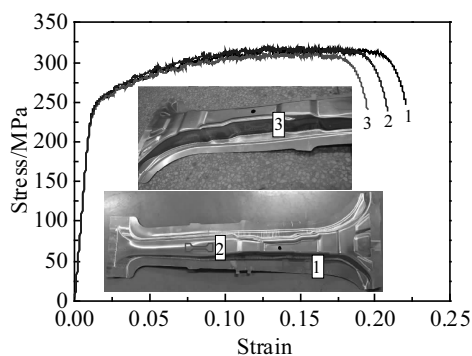


Fig.7 Engineering stress-strain curves at different locations

Harrison's<sup>[33]</sup> work. It is demonstrated that the BP neural network can accurately reveal the nonlinear relationship between hot stamping process parameters and formability. The GA can effectively search the optimal process parameters for excellent formability. The combination of BP and GA is effective in the optimization of hot stamping process parameters.

#### 4 Conclusions

1) Satisfactory formability of the hot stamping aluminum alloy B-pillar confirms the validity of the BP-GA method, which can be generally used in the optimization of hot stamping process parameters.

2) The FE model established in this study can accurately simulate the actual hot stamping process of complex 6061 aluminum alloy components by employing the unified viscoplastic damage constitutive equations. The FE simulation results match well with the experimental results, and the maximum relative error between them is only 1.9%.

3) A satisfactory B pillar (1:1 with the actual one in size) with good formability and little springback is achieved using the optimized results. Combining the BP neural network with multi-objective genetic algorithm, the optimum parameters for AA6061 hot stamping process are a blank temperature of 386 °C, a stamping speed of 286 mm/s and a clearance of 1.84 mm. The maximum thinning rate and thickening rate are only 13.0% and 10.0%, respectively.

#### References

- Zhang Jing, Yang Liang, Zuo Rulin. *Rare Metal Materials and Engineering*[J], 2015, 44(4): 956 (in Chinese)
- Zhang J X, Zhang K L, Liu Y T et al. *Rare Metals*[J], 2014, 33(4): 404
- Zhang J X, Fan J X, Liu Y T et al. *Rare Metals*[J], 2015, 34(6): 387
- Hu Z L, Wang X S, Pang Q et al. *International Journal of Advanced Manufacturing Technology*[J], 2015, 80(5-8): 959
- Fan X B, Zhu-Bin H E. *Transactions of Nonferrous Metals Society of China*[J], 2012, 22: S389
- Toros S, Ozturk F, Kacar I. *Journal of Materials Processing Technology*[J], 2008, 207(1-3): 1
- Mahabunphachai S, Koç M. *Materials & Design*[J], 2010, 31(5): 2422
- Golovashchenko S, Krause A. *Journal of Materials Engineering & Performance*[J], 2005, 14(4): 503
- Kleiner M, Geiger M, Klaus A. *CIRP Annals-Manufacturing Technology*[J], 2003, 52(2): 521
- Lin J, Dean TA, Garrett R P et al. *UK Patent*, WO/2008/059242[P], 2008
- Fan X, He Z, Zheng K et al. *Materials & Design*[J], 2015, 83: 557
- Foster A D, Mohamed M S, Lin J et al. *Steel Research International*[J], 2008, 79(2): 113

- 13 Mohamed M S. An Investigation of Hot Forming Quench Process for AA6082 Aluminium Alloys[D]. London: Imperial College London, 2010
- 14 Fan X, He Z, Yuan S et al. Materials Science & Engineering A[J], 2013, 573(18): 154
- 15 Fan X B, He Z B, Zhou W X et al. Journal of Materials Processing Technology[J], 2016, 228: 179
- 16 Wang L, Strangwood M, Balint D et al. Materials Science & Engineering A[J], 2011, 528(6): 2648
- 17 Ma W Y, Wang B Y, Lei F U et al. Transactions of Nonferrous Metals Society of China[J], 2015, 25(7): 2342
- 18 Zhou Jing, Wang Baoyu, Lin Jianguo et al. Archives of Civil and Mechanical Engineering[J], 2013, 13(3): 401
- 19 Xiao W, Wang B, Zhou J et al. Engineering Optimization[J], 2016, 48(12): 2173
- 20 Park D H, Ko B C, Yoo Y C. Journal of Materials Science[J], 2002, 37(8): 1593
- 21 Soundararajan V, Zekovic S, Kovacevic R. International Journal of Machine Tools & Manufacture[J], 2005, 45(14): 1577
- 22 Lin J. Fundamentals of Material Modelling for Metals Processing Technologies[M]. London: Imperial College Press, 2015
- 23 Mohamed S M, Foster A D, Lin J G et al. International Journal of Machine Tools & Manufacture[J], 2012, 53(1): 27
- 24 Ma W, Wang B, Bian J et al. Metallurgical & Materials Transactions A[J], 2015, 46(6): 2748
- 25 Lorenz D. Simulation of Thermo-Mechanical Forming Process with LS-DYNA[M]. Bamberg: LS-DYNA Forum, 2010
- 26 Zhou J, Wang B Y, Lin J G et al. Transactions of Nonferrous Metals Society of China[J], 2014, 24(11): 3611
- 27 Karbasian H, Tekkaya A E. Journal of Materials Processing Technology[J], 2010, 210(15): 2103
- 28 Younesi M, Bahrololoom M E, Ahmadzadeh M. Computational Materials Science[J], 2010, 47(3): 645
- 29 Fu Z, Mo J, Chen L et al. Materials & Design[J], 2010, 31(1): 267
- 30 Dehghani K, Nekahi A. Materials & Design[J], 2010, 31(4): 2224
- 31 Yu W, Li M Q, Luo J et al. Materials & Design[J], 2010, 31(7): 3282
- 32 Li W, Zhan L, Zhao J. The Chinese Journal of Nonferrous Metals[J], 2016, 26(6): 1159 (in Chinese)
- 33 Harrison N R, Luckey S G. Sae International Journal of Materials & Manufacturing[J], 2014, 7(3): 567

## 铝合金复杂汽车零部件热成形-淬火一体化工艺参数优化

李欢欢<sup>1,2,3</sup>, 胡志力<sup>2,3</sup>, 华林<sup>1,2,3</sup>, 陈一哲<sup>2,3</sup>

(1. 武汉理工大学 材料科学与工程学院, 湖北 武汉 430070)

(2. 武汉理工大学 现代汽车零部件技术湖北省重点实验室, 湖北 武汉 430070)

(3. 武汉理工大学 汽车零部件技术湖北省协同创新中心, 湖北 武汉 430070)

**摘要:** 铝合金热成形-淬火一体化工艺将成形和热处理结合, 能同时实现零件尺寸精度和性能的控制, 是实现汽车轻量化的主要途径之一。但是在冲压成形尺寸相对较大、形状相对较复杂的铝合金板件时, 依然存在各工艺参数难调试的问题。建立了 AA6061 铝合金的热变形统一黏塑性损伤本构模型, 将其用于铝合金汽车 B 柱热冲压成形模拟, 采用 BP 神经网络构建了工艺参数 (板料成形温度, 冲压速度, 模具间隙) 与成形性 (最大减薄率, 最大增厚率) 之间的关系并结合遗传算法实现多目标优化, 得到了 AA6061 铝合金热冲压的最佳成形工艺参数。优化之后, B 柱的最大减薄率和最大增厚率分别从 56.5% 和 14.2% 降到了 13.0% 和 10.0%, 通过优化之后的工艺参数, 制得了成形性良好、尺寸精度高的零件。结果证明了基于神经网络和遗传算法的热成形工艺优化方法的可行性和有效性。

**关键词:** 热冲压; 统一黏塑性损伤本构模型; BP 神经网络; 多目标优化

作者简介: 李欢欢, 女, 1989 年生, 博士生, 武汉理工大学材料科学与工程学院, 湖北 武汉 430070, 电话: 027-87168391, E-mail: cherielisky@163.com